

High-Temperature Superconductivity in Th-H System at Pressure Conditions

Alexander G. Kvashnin,^{1,2} Dmitry V. Semenov,^{1,2} Ivan A. Kruglov,^{2,3} Artem R. Oganov,^{1,2,3,4}

¹ Skolkovo Institute of Science and Technology, Skolkovo Innovation Center 143026, 3 Nobel Street, Moscow, Russian Federation

² Moscow Institute of Physics and Technology, 141700, 9 Institutsky lane, Dolgoprudny, Russian Federation

³ Dukhov Research Institute of Automatics (VNIIA), Moscow 127055, Russian Federation

⁴ International Center for Materials Discovery, Northwestern Polytechnical University, Xi'an, 710072, China

Corresponding Author

*A.G. Kvashnin, E-mail: A.Kvashnin@skoltech.ru.

ABSTRACT. Several new thorium hydrides were predicted to be stable under pressure using evolutionary algorithm USPEX, including ThH₃, Th₃H₁₀, ThH₄, ThH₆, ThH₇ and ThH₁₀. Superconducting properties of all predicted phases were studied. The highest calculated superconducting transition temperature T_C was found to be 194 K at 100 GPa for the newly predicted *Fm* $\bar{3}$ *m*-ThH₁₀. We discuss the potential of further investigation of new actinide-based hydrides in order to find new high-temperature superconductors.

Introduction

Thorium is a weakly radioactive element, its most stable isotope ²³²Th having a half-life of 14 billion years. Thorium belongs to the actinide series, but its physical and chemical properties are mainly dictated by 6*d* electrons, similar to transition metals Ti, Hf, or Zr.¹ Bulk thorium has fcc structure (*Fm* $\bar{3}$ *m* space group) in contrast to other elements of actinide series.² Thorium is a weak BCS (Bardeen-Cooper-Schrieffer) type-I superconductor with T_C = 1.374 K^{2,3} and with a critical magnetic field H_C = 15.92 mT.^{4,2} Theoretical predictions of the electron–phonon coupling have been reported to be in good agreement with experimental data.^{5–7}

Thorium oxide ThO₂ is widely used as a stabilizer in tungsten alloys, as possible catalyst and in gas lighting devices. Thorium reacts with hydrogen to form hydrides ThH₂ and Th₄H₁₅, the latter being the first known superconducting hydride with metallic conductivity at normal conditions, and its superconducting T_C = 7.5–8 K.^{8,9} They are chemically active and readily decompose upon exposure to air or moisture.¹⁰ Stability and electronic properties of ThH₂ and Th₄H₁₅ were studied theoretically.^{11,12}

Unexpected effect of thorium doping on GdFeAsO (Gd_(1-x)Th_xFeAsO) was studied by Wang et al.¹³ Doping by 20% of thorium leads to increase of the T_C from 36 to 56 K. Investigations of superconducting properties of thorium hydrides and deuterides revealed the absence of the isotope effect in Th₄H₁₅, which makes possible to consider this material as a superconductor without predominant electron-phonon pairing mechanism.

Recent experimental and theoretical studies of different hydrogen-rich hydrides show that some of them are high-temperature superconductors under pressure.^{14–21} Moreover, recent theoretical investigations of uranium²², lanthanum and yttrium hydrides under pressure indicate possible existence of exceptional high-temperature, maybe even room-temperature superconductivity²³. All these studies motivated us to perform a systematic evolutionary search for new phases in the Th-H system at pressure in the range from 0 to 200 GPa. As we show below, one of the new hydrides is predicted to be a high-temperature superconductor.

Computational Methodology

Evolutionary algorithm USPEX^{24–26} is a powerful tool for predicting thermodynamically stable compounds of given elements at a given pressure. We performed variable-composition

searches in the Th-H system at pressures 0, 50, 100, 150 and 200 GPa. The first generation (120 structures) was created using random symmetric generator, while all subsequent generations contained 20% random structures, and 80% created using heredity, softmutation and transmutation operators. Here, evolutionary searches were combined with structure relaxations using density functional theory (DFT)^{27,28} within the generalized gradient approximation (Perdew-Burke-Ernzerhof functional),²⁹ and the projector augmented wave method^{30,31} as implemented in the VASP code.³²⁻³⁴ Plane wave kinetic energy cutoff was set to 600 eV and the Brillouin zone was sampled by Γ -centered k-points meshes with resolution $2\pi \times 0.05 \text{ \AA}^{-1}$.

In order to establish stability fields of the predicted phases, we recalculated their enthalpies with increased precision at various pressures with a smaller pressure increment (from 5 to 10 GPa), recalculating the thermodynamic convex hull (Maxwell construction) at each pressure. By definition, a thermodynamically stable phase has lower Gibbs free energy (or, at zero Kelvin, lower enthalpy) than any phase or phase assemblage of the same composition. Thus, phases that were located on the convex hull are the ones stable at given pressure. Stable structures of elemental Th and H were taken from USPEX calculations and from Refs.³⁵ and ³⁶, respectively.

Calculations of superconducting T_C were carried out using QUANTUM ESPRESSO package³⁷. Phonon frequencies and electron-phonon coupling (EPC) coefficients were computed using density-functional perturbation theory³⁸, employing plane-wave pseudopotential method and Perdew-Burke-Ernzerhof exchange-correlation functional²⁹. Convergence tests showed that 120 Ry is a suitable kinetic energy cutoff for the plane wave basis set. Electronic band structures of newly found thorium hydrides were calculated using both VASP and QE, and demonstrated good consistency. Comparison of the phonon densities of states calculated using finite displacement method (VASP and PHONOPY^{39,40}) and density-functional perturbation theory (QE) showed perfect agreement between these methods.

In our calculations of the electron-phonon coupling (EPC) parameter λ , the first Brillouin zone was sampled using $4 \times 4 \times 4$ q-points mesh, and a denser $16 \times 16 \times 16$ k-points mesh (with Gaussian smearing and $\sigma = 0.02$ Ry, which approximates the zero-width limits in the calculation of λ). The superconducting transition temperature T_C was estimated by using two equations: "full" – Allen-Dynes and "short" – modified McMillan equation.⁴¹ The "full" Allen-Dynes equation for calculating T_C has the following form:⁴¹

$$T_C = \omega_{log} \frac{f_1 f_2}{1.2} \exp\left(\frac{-1.04(1 + \lambda)}{\lambda - \mu^* - 0.62\lambda\mu^*}\right), \quad (1)$$

while the modified McMillan equation has the form as:

$$T_C = \frac{\omega_{log}}{1.2} \exp\left(\frac{-1.04(1 + \lambda)}{\lambda - \mu^* - 0.62\lambda\mu^*}\right). \quad (2)$$

The EPC constant λ and logarithmic average frequency ω_{log} were calculated as:

$$\lambda = \int_{\omega_{min}}^{\omega_{max}} \frac{2 \cdot \alpha^2 F(\omega)}{\omega} d\omega \quad (3)$$

and

$$\omega_{log} = \exp\left(\frac{2}{\lambda} \int_{\omega_{min}}^{\omega_{max}} \frac{d\omega}{\omega} \alpha^2 F(\omega) \ln(\omega)\right), \quad (4)$$

and μ^* is the Coulomb pseudopotential, for which we used widely accepted lower and upper bound values of 0.10 and 0.15.

Crystal structures of predicted phases were visualized using VESTA software.⁴²

Results

We built the composition-pressure phase diagram (see Fig. 1), which shows pressure ranges of stability of all found phases at different pressures. As shown in Fig. 1, our calculations correctly reproduce stability of ThH_2 and Th_4H_{15} phases and predict 8 new stable phases namely $R\bar{3}m$ -

ThH₃, *Immm*-Th₃H₁₀, *Pnma*-ThH₄, *P321*-ThH₄, *I4/mmm*-ThH₄, *Cmc2*₁-ThH₆, *P2*₁/*c*-ThH₇ and *Fm* $\bar{3}$ *m*-ThH₁₀.

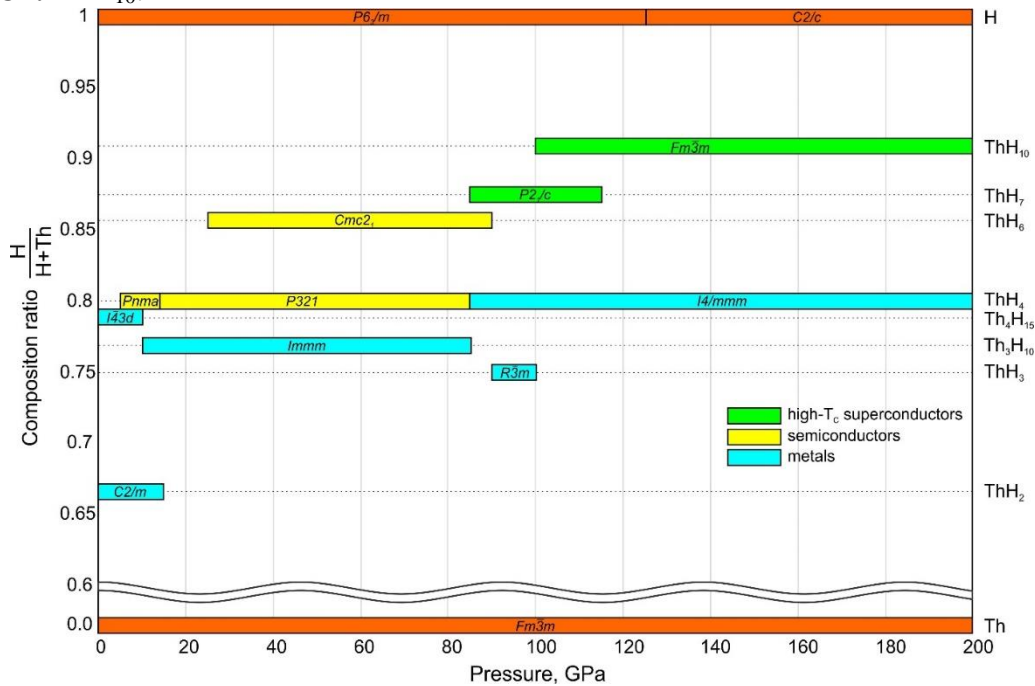


Fig. 1 Pressure-composition phase diagram of the Th-H system. Yellow, blue and green indicate semiconducting, normal metallic and high- T_C superconducting phases, respectively.

It is clearly seen from our calculations that at the pressure of 5 GPa the new semiconducting *Pnma*-ThH₄ phase becomes stable while increasing pressure leads to the phase transition to another semiconducting *P321*-ThH₄ at about 15 GPa. Further increase of pressure leads to the *P321* \rightarrow *I4/mmm* phase transition at 90 GPa. At the pressure of 10 GPa, the *Immm*-Th₃H₁₀ phase becomes thermodynamically stable and remains stable up to 90 GPa. *Cmc2*₁-ThH₆ phase appears on the phase diagram in the pressure range 25-90 GPa. The *R* $\bar{3}$ *m*-ThH₃ phase is stable in a very narrow pressure range from 90 to 100 GPa. At pressures higher than 100 GPa only 3 phases are stable namely *I4/mmm*-ThH₄, *P2*₁/*c*-ThH₇ and *Fm* $\bar{3}$ *m*-ThH₁₀. The *I4/mmm*-ThH₄ and *Fm* $\bar{3}$ *m*-ThH₁₀ phases are stable up to 200 GPa, while the *P2*₁/*c*-ThH₇ is unstable at pressures higher than 120 GPa.

It is important to note that three of predicted Th-H phases are semiconductors (yellow color in Fig. 1) with the DFT band gaps around 1 eV; the systematic underestimation of the band gap by DFT-PBE method is well known. The rest of predicted phases *R* $\bar{3}$ *m*-ThH₃, *Immm*-Th₃H₁₀, *I4/mmm*-ThH₄, *P2*₁/*c*-ThH₇ and *Fm* $\bar{3}$ *m*-ThH₁₀ are metallic and are potential high-temperature superconductors. Crystal structures of ThH₇ and ThH₁₀ are shown in Fig. 2. The *P2*₁/*c*-ThH₇ phase has thorium atoms forming a bcc sublattice; each thorium atom has irregular coordination by hydrogen atoms. (see Fig. 2). Thorium coordination number is remarkably high (23), distances are in the range from 2.03 to 2.23 Å at 100 GPa. We observe high DOS at the Fermi level, which also should be favorable for superconducting properties. *Fm* $\bar{3}$ *m*-ThH₁₀ is isostructural to lanthanum hydride phase LaH₁₀ from Ref. ²³, but *Fm* $\bar{3}$ *m*-ThH₁₀ is stable at lower pressures (> 100 GPa versus > 150 GPa for LaH₁₀).

Phonon calculations confirmed that all newly predicted superconducting phases have no imaginary phonon frequencies in their predicted ranges of thermodynamic stability (see Fig. 2). Structures of *R* $\bar{3}$ *m*-ThH₃, *Immm*-Th₃H₁₀, *I4/mmm*-ThH₄ phases are shown in Fig. S1 (see Supporting Information).

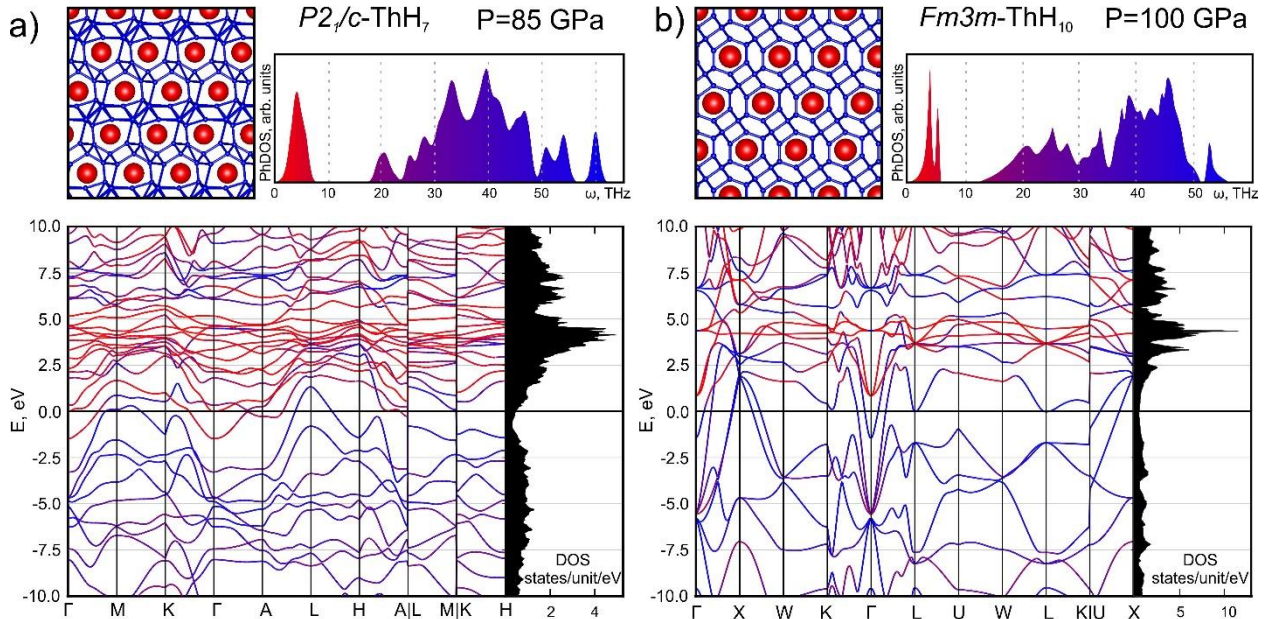


Fig. 2 Crystal structure, phonon density of states, electronic band structure and density of states for predicted a) $P2_1/c$ -ThH₇ and b) $Immm$ -ThH₁₀ phases.

In the BSC theory of superconductivity, the main quantity is the electron-phonon coupling (EPC) coefficient λ . The superconducting transition temperature (T_C) can be calculated using “full” Allen-Dynes formula (see Eq. (1)) or the Allen-Dynes modified McMillan formula (see Eq. (2)) where for the Coulomb pseudopotential μ^* we used the commonly accepted bracketing values of 0.10 and 0.15. Detailed information on the calculated superconducting properties of thorium hydrides is given in Table 1.

As we mentioned above, the following new phases are metallic and potentially superconducting: $R\bar{3}m$ -ThH₃, $Immm$ -Th₃H₁₀, $I4/mmm$ -ThH₄, $P2_1/c$ -ThH₇ and $Fm\bar{3}m$ -ThH₁₀. For $Fm\bar{3}m$ -ThH₁₀ at 100 GPa, the EPC coefficient $\lambda = 2.19$ and the eq. (1) with adjustment factors f_1 and f_2 was used for calculation T_C . Transition temperature was calculated to be in a range from 165 to 195 K (depending on the exact μ^* value). For $P2_1/c$ -ThH₇ at 100 GPa, we find a much lower EPC coefficient of 0.84, resulting in a much lower (but still high) T_C in the range 43-61 K (see Table 1). However, $R\bar{3}m$ -ThH₃ cannot be considered as superconductor due to the very low EPC coefficient of 0.11 leading to T_C close to 0 K. Calculated T_C for the low-pressure metallic $Immm$ -Th₃H₁₀ phase equals 4 K and is caused by weak electron-phonon interaction ($\lambda = 0.48$, $\omega_{log} = 380$ K, see Table 1). The $I4/mmm$ -ThH₄ phase shows low T_C of ~ 3 K along with weak electron-phonon coupling ($\lambda = 0.36$). The strong dependence of the T_C on the amount of hydrogen in hydrides is mostly due to higher EPC resulting from covalent Th-H and H-H bonds.

Table 1. Predicted superconducting properties of thorium hydrides. T_C values are given for μ^* equal to 0.1, while T_C in brackets are for $\mu^* = 0.15$.

Phase	P , GPa	λ	N_β states/unit/eV	ω_{log} , K	T_C (Allen-Dynes), K	T_C (McMillan), K
$R\bar{3}m$ -ThH ₃	100	0.11	0.76	1663.9	~ 0	~ 0
$Immm$ -Th ₃ H ₁₀	10	0.48	3.89	378.6	3.9 (1.2)	3.8 (1.2)
$I4/mmm$ - ThH ₄	85	0.36	0.56	1003.0	3.0 (0.5)	2.97 (0.5)
$P2_1/c$ -ThH ₇	100	0.84	0.57	1192.0	64.8 (45.3)	61.4 (43.4)
	100	2.19	0.61	1042.8	194.4 (159.3)	168.5 (142.9)
$Fm\bar{3}m$ -ThH ₁₀	200	1.58	0.53	1215.8	163.0 (137.4)	145.2 (125.0)
	300	0.99	0.48	1728.5	126.4 (95.3)	118.5 (90.5)

As the $Fm\bar{3}m$ -ThH₁₀ phase is stable in a wide range of pressures, we determined the main parameters responsible for superconducting properties as a function of pressure (see Fig. 3). We

calculated the Eliashberg function $a^2F(\omega)$ as a function of pressure (Fig. 3a). One can note, that increase of pressure leads to shifting of $a^2F(\omega)$ function to high frequencies. Calculated EPC coefficient λ and ω_{\log} as a function of external pressure are shown in Fig. 3b. Here one can note as the EPC coefficient decreases with the pressure, while the ω_{\log} increases linearly. One can see the pronounced linear dependence of T_C on the external pressure (see Fig. 3c).

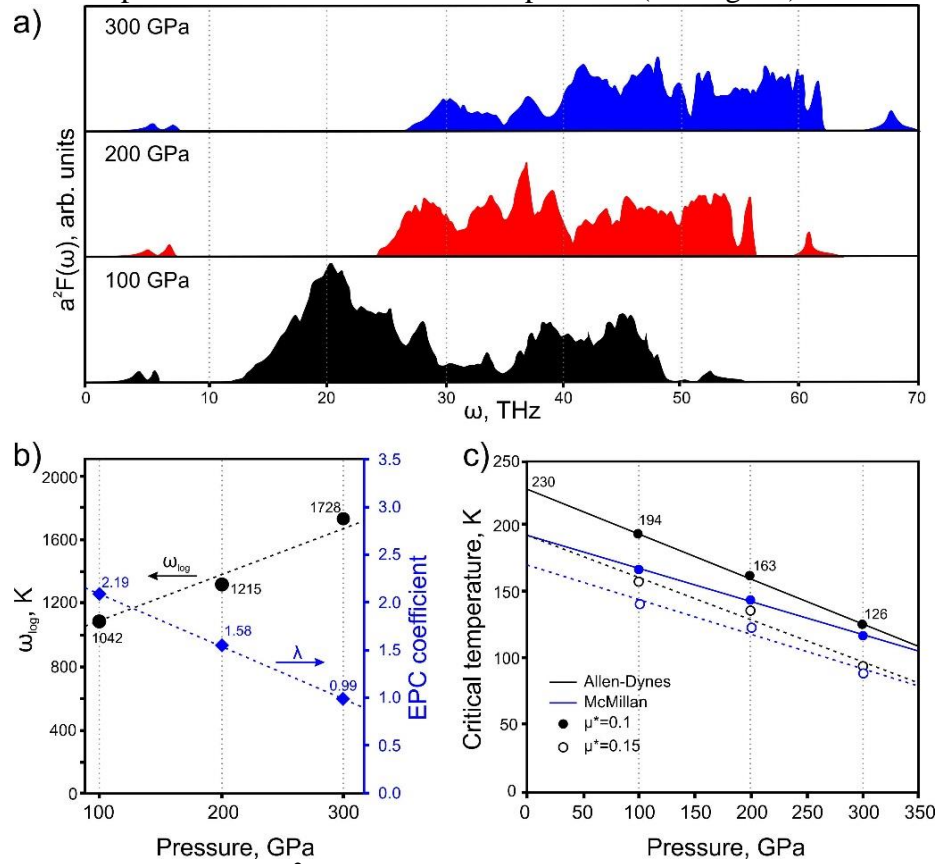


Fig. 3. a) Eliashberg function $a^2F(\omega)$, b) ω_{\log} and EPC coefficient λ , c) critical transition temperature (T_C) of $Fm\bar{3}m$ -ThH₁₀ as a function of pressure.

These results can be analyzed by the well-known empirical equation for low- T_C superconductors^{43,44} $-\ln\left(\frac{T_C}{\omega_{\log}}\right) = Cv^{-\phi}$, $C > 0$, where v is unit cell volume (see Supporting Information for details). The computed pressure coefficient $dT_C/dP = -0.35$ K/GPa (at 100 GPa) is close to the value for CaH₆ (-0.33 K/GPa⁴⁵). However, this dT_C/dP is only half that of UH₈ (-0.69 K/GPa²²), which can be explained by higher electronic density of states at Fermi level in UH₈ (see Supporting information for details).

Conclusions

In conclusion, we studied Th-H system using global optimization algorithm USPEX in order to predict new superconducting thorium hydrides, exploring pressures up to 200 GPa. Two new high-temperature superconductors were predicted, namely $Fm\bar{3}m$ -ThH₁₀ and $P2_1/c$ -ThH₇. $Fm\bar{3}m$ -ThH₁₀ is predicted to be superconducting at temperature up to 194 K at 100 GPa. It was found that critical temperature of transition to superconducting state for considered hydrides increases nonlinearly as the amount of hydrogen increases. This result is in agreement with the idea of reaching room- T_C for BCS superconductors by increasing the amount of hydrogen in compounds. Our ThH₁₀ is one of the highest- T_C superconductors discovered so far. A reasonable step after exhausting all binary hydrides is to pay more attention to systems of higher complexity, primarily to ternary A-B-H systems.

Acknowledgements

The work was supported by Russian Science Foundation (№ 16-13-10459). Calculations were performed on the Rurik supercomputer at MIPT. Authors thank Dr. Linu Malakkal for providing pseudopotential for thorium.

References

1. Cunningham, B. B. & Wallmann, J. C. Crystal structure and melting point of curium metal. *J. Inorg. Nucl. Chem.* **26**, 271–275 (1964).
2. Griveau, J.-C. & Colineau, É. Superconductivity in transuranium elements and compounds. *Comptes Rendus Phys.* **15**, 599–615 (2014).
3. Müller, W. *et al.* The electrical resistivity and specific heat of americium metal. *J. Low Temp. Phys.* **30**, 561–578 (1978).
4. Decker, W. R. & Finnemore, D. K. Critical-Field Curves for Gapless Superconductors. *Phys. Rev.* **172**, 430–436 (1968).
5. Skriver, H. L. & Mertig, I. Electron-phonon coupling of the actinide metals. *Phys. Rev. B* **32**, 4431–4441 (1985).
6. Allen, P. B. Empirical electron-phonon lambda values from resistivity of cubic metallic elements. *Phys. Rev. B* **36**, 2920–2923 (1987).
7. Skriver, H. L., Eriksson, O., Mertig, I. & Mrosan, E. Electron-phonon coupling in the actinides. *Phys. Rev. B* **37**, 1706–1710 (1988).
8. Dietrich, M., Gey, W., Rietschel, H. & Satterthwaite, C. B. Pressure dependence of the superconducting transition temperature of Th₄H₁₅. *Solid State Commun.* **15**, 941–943 (1974).
9. Wickleder, M. S., Fourest, B. & Dorhout, P. K. Thorium. in *The Chemistry of the Actinide and Transactinide Elements* 52–160 (Springer, Dordrecht, 2008). doi:10.1007/1-4020-3598-5_3
10. Greenwood, N. N. & Earnshaw, A. *Chemistry of the elements*. (Pergamon Press, 1984).
11. Weaver, J. H., Knapp, J. A., Eastman, D. E., Peterson, D. T. & Satterthwaite, C. B. Electronic Structure of the Thorium Hydrides ThH₂ and Th₄H₁₅. *Phys. Rev. Lett.* **39**, 639–642 (1977).
12. Shein, I. R., Shein, K. I., Medvedeva, N. I. & Ivanovskii, A. L. Electronic band structure of thorium hydrides: ThH₂ and Th₄H₁₅. *Phys. B Condens. Matter* **389**, 296–301 (2007).
13. Wang, C. *et al.* Thorium-doping-induced superconductivity up to 56 K in Gd_(1-x)Th_xFeAsO. *EPL Europhys. Lett.* **83**, 67006 (2008).
14. Gao, G. *et al.* Superconducting High Pressure Phase of Germane. *Phys. Rev. Lett.* **101**, 107002 (2008).
15. Gao, G. *et al.* High-pressure crystal structures and superconductivity of Stannane (SnH₄). *Proc. Natl. Acad. Sci.* **107**, 1317–1320 (2010).
16. Duan, D. *et al.* Pressure-induced metallization of dense (H₂S)₂H₂ with high-T_c superconductivity. *Sci. Rep.* **4**, 6968 (2014).
17. Hou, P. *et al.* High pressure structures and superconductivity of AlH₃(H₂) predicted by first principles. *RSC Adv.* **5**, 5096–5101 (2015).
18. Li, Y. *et al.* Pressure-stabilized superconductive yttrium hydrides. *Sci. Rep.* **5**, srep09948 (2015).
19. Goncharov, A. F. *et al.* Hydrogen sulfide at high pressure: Change in stoichiometry. *Phys. Rev. B* **93**, 174105 (2016).
20. Esfahani, M. M. D. *et al.* Superconductivity of novel tin hydrides (Sn_nH_m) under pressure. *Sci. Rep.* **6**, srep22873 (2016).
21. Durajski, A. P. & Szczyński, R. First-principles study of superconducting hydrogen sulfide at pressure up to 500 GPa. *Sci. Rep.* **7**, 4473 (2017).
22. Kruglov, I. A. *et al.* High-temperature superconductivity of uranium hydrides at near-ambient conditions. *arXiv:1708.05251* <https://arxiv.org/abs/1708.05251>, (2017).
23. Liu, H., Naumov, I. I., Hoffmann, R., Ashcroft, N. W. & Hemley, R. J. Potential high-T_C superconducting lanthanum and yttrium hydrides at high pressure. *Proc. Natl. Acad. Sci.* 201704505 (2017). doi:10.1073/pnas.1704505114
24. Oganov, A. R. & Glass, C. W. Crystal structure prediction using ab initio evolutionary techniques: Principles and applications. *J Chem Phys* **124**, 244704 (2006).
25. Oganov, A. R., Lyakhov, A. O. & Valle, M. How Evolutionary Crystal Structure Prediction Works—and Why. *Acc. Chem. Res.* **44**, 227–237 (2011).
26. Lyakhov, A. O., Oganov, A. R., Stokes, H. T. & Zhu, Q. New developments in evolutionary structure prediction algorithm USPEX. *Comput. Phys. Commun.* **184**, 1172–1182 (2013).
27. Hohenberg, P. & Kohn, W. Inhomogeneous electron gas. *Phys Rev* **136**, B864–B871 (1964).
28. Kohn, W. & Sham, L. J. Self-consistent equations including exchange and correlation effects. *Phys Rev* **140**, A1133–A1138 (1965).
29. Perdew, J. P., Burke, K. & Ernzerhof, M. Generalized gradient approximation made simple. *Phys. Rev. Lett.* **77**, 3865–3868 (1996).
30. Blöchl, P. E. Projector augmented-wave method. *Phys. Rev. B* **50**, 17953–17979 (1994).

31. Kresse, G. & Joubert, D. From ultrasoft pseudopotentials to the projector augmented-wave method. *Phys. Rev. B* **59**, 1758–1775 (1999).
32. Kresse, G. & Furthmüller, J. Efficient iterative schemes for ab initio total-energy calculations using a plane-wave basis set. *Phys. Rev. B* **54**, 11169–11186 (1996).
33. Kresse, G. & Hafner, J. Ab initio molecular dynamics for liquid metals. *Phys. Rev. B* **47**, 558–561 (1993).
34. Kresse, G. & Hafner, J. Ab initio molecular-dynamics simulation of the liquid-metal amorphous-semiconductor transition in germanium. *Phys. Rev. B* **49**, 14251–14269 (1994).
35. Evans, D. S. & Raynor, G. V. The lattice spacing of thorium, with reference to contamination. *J. Nucl. Mater.* **1**, 281–288 (1959).
36. Pickard, C. J. & Needs, R. J. Structure of phase III of solid hydrogen. *Nat. Phys.* **3**, 473–476 (2007).
37. Giannozzi, P. *et al.* QUANTUM ESPRESSO: a Modular and Open-Source Software Project for Quantum Simulations of Materials. *J. Phys. Condens. Matter* **21**, 395502 (2009).
38. Baroni, S., de Gironcoli, S., Dal Corso, A. & Giannozzi, P. Phonons and Related Crystal Properties from Density-Functional Perturbation Theory. *Rev. Mod. Phys.* **73**, 515–562 (2001).
39. Togo, A. & Tanaka, I. First principles phonon calculations in materials science. *Scr. Mater.* **108**, 1–5 (2015).
40. Togo, A., Oba, F. & Tanaka, I. First-principles calculations of the ferroelastic transition between rutile-type and CaCl₂-type SiO₂ at high pressures. *Phys. Rev. B* **78**, 134106 (2008).
41. Allen, P. B. & Dynes, R. C. Transition temperature of strong-coupled superconductors reanalyzed. *Phys. Rev. B* **12**, 905–922 (1975).
42. Momma, K. & Izumi, F. VESTA 3 for three-dimensional visualization of crystal, volumetric and morphology data. *J. Appl. Crystallogr.* **44**, 1272–1276 (2011).
43. Rohrer, H. Druck- und Volumeneffekte in der Supraleitung. *Helv Phys Acta* **33**, 675–705 (1960).
44. Olsen, J. L. & Rohrer, H. The volume dependence of the electron level density and the critical temperature in superconductors. *Helv Phys Acta* **33**, 872–880 (1960).
45. Wang, H., Tse, J. S., Tanaka, K., Iitaka, T. & Ma, Y. Superconductive sodalite-like clathrate calcium hydride at high pressures. *Proc. Natl. Acad. Sci.* **109**, 6463–6466 (2012).

Supporting Information. High-Temperature Superconductivity in Th-H System at Pressure Conditions

Alexander G. Kvashnin,^{1,2} Dmitry V. Semenov,^{1,2} Ivan A. Kruglov,^{2,3} Artem R. Oganov,^{1,2,3,4}

¹ Skolkovo Institute of Science and Technology, Skolkovo Innovation Center 143026, 3 Nobel Street, Moscow, Russian Federation

² Moscow Institute of Physics and Technology, 141700, 9 Institutsky lane, Dolgoprudny, Russian Federation

³ Dukhov Research Institute of Automatics (VNIIA), Moscow 127055, Russian Federation

⁴ International Center for Materials Discovery, Northwestern Polytechnical University, Xi'an, 710072, China

Crystal data of Th-H phases.....	9
Equations for calculation T_C	9
Electronic properties of Th-H phases.....	10
Eliashberg spectral functions for ThH ₃ , Th ₃ H ₁₀ and ThH ₇ phases	12
Dependence of T_C on the pressure for ThH ₁₀ and UH ₈ phases.....	13
References.....	15

Crystal data of Th-H phases

It can be seen from Fig. S4a that $R\bar{3}m$ -ThH₃ phase has a layered structure, where Th atoms occupy (0,0,0) positions and hydrogen atoms are in between thorium layers. Coordination number of thorium in this structure equals to 14 and distance between Th and H ($d(\text{Th-H})$) equals to 2.1 Å at 90 GPa (see Fig. S4a). The shortest distance between hydrogen atoms in the layer is 1.8 Å, so they do not form a chemical bond in $R\bar{3}m$ -ThH₃. Layered structure of $R\bar{3}m$ -ThH₃ phase directly impacts on the electronic properties. Flat bands are seen in the $\Gamma \rightarrow A$, $L \rightarrow M$ and $K \rightarrow H$ directions, which are perpendicular to the layers. The electronic density at Fermi level mainly comes from thorium atoms (red bands in Fig. S4a). The crystal structure of $Im\bar{m}m$ -Th₃H₁₀ phase contains 12-coordinate thorium atoms in the bcc arrangement (with Th-H distance of 2.28 Å at 10 GPa) and hydrogen atoms laying along the [1,0,0], [0,1,0] and [0,0,1] planes (see Fig. S4b). ThH₄ phase has orthorhombic lattice with thorium atoms in (0,0,0) positions. Each thorium atom is surrounded by 12 hydrogen atoms (see Fig. S4c). The H-H distance varies from 1.57 to 1.65 Å.

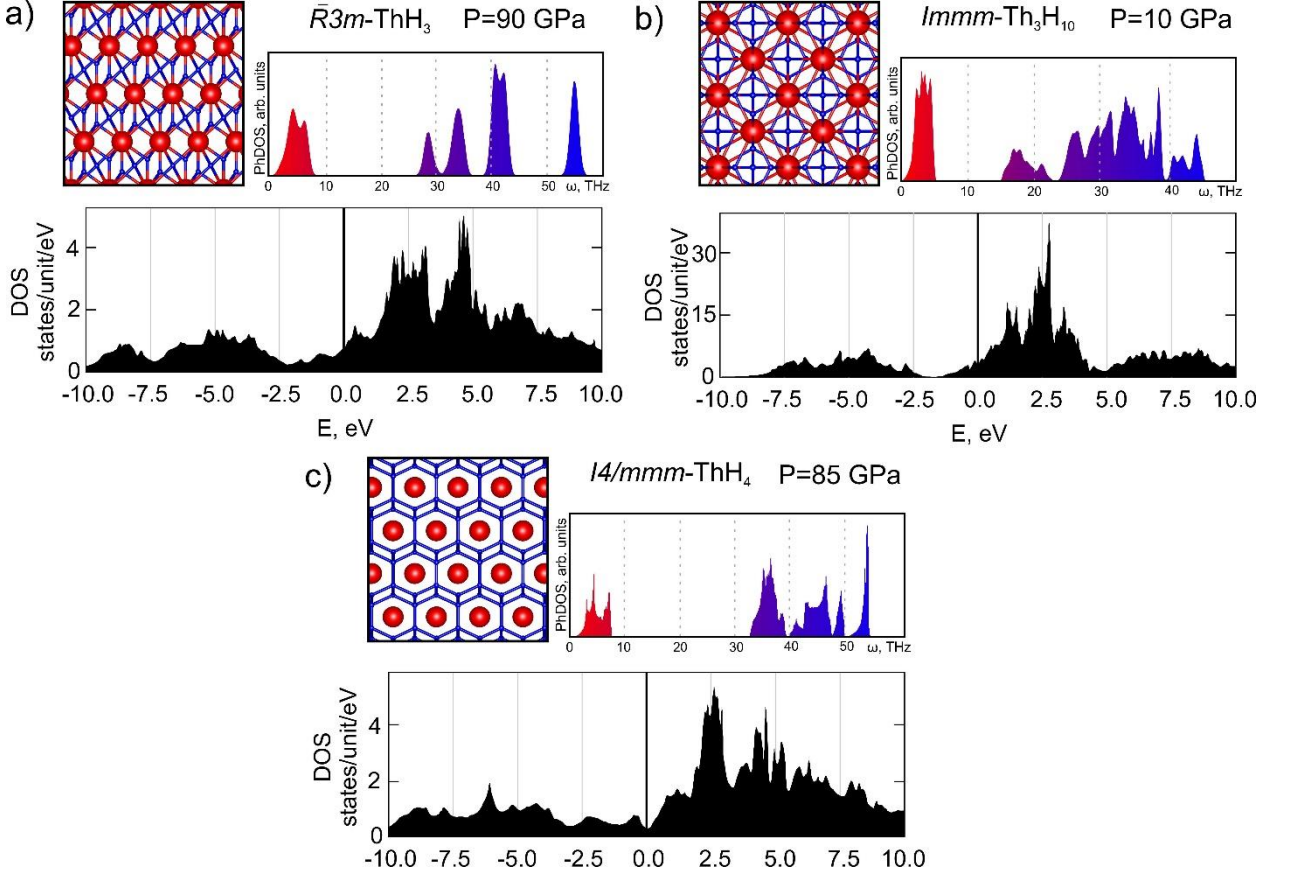


Fig. S4. Crystal structure, phonon density of states, electronic band structure and density of states for predicted a) $R\bar{3}m$ -ThH₃, b) $Im\bar{m}m$ -Th₃H₁₀ and c) $I4/m\bar{m}m$ -ThH₄ phases.

Equations for calculation T_C

The “full” Allen-Dynes equation for calculating T_C has the following form [1]:

$$T_C = \omega_{log} \frac{f_1 f_2}{1.2} \exp\left(\frac{-1.04(1 + \lambda)}{\lambda - \mu^* - 0.62\lambda\mu^*}\right), \quad (S5)$$

while the modified McMillan equation has the form as:

$$T_C = \frac{\omega_{log}}{1.2} \exp\left(\frac{-1.04(1 + \lambda)}{\lambda - \mu^* - 0.62\lambda\mu^*}\right), \quad (S6)$$

where

$$f_1 = \left(1 + \left(\frac{\lambda}{\Lambda_1}\right)^{\frac{3}{2}}\right)^{\frac{1}{3}}, \quad f_2 = 1 + \frac{\lambda^2}{\lambda^2 + \Lambda_2^2} \cdot \left(\frac{\omega_2}{\omega_{log}} - 1\right) \quad (\text{S7})$$

and

$$\Lambda_1 = 2.46(1 + 3.8\mu^*), \quad \Lambda_2 = 1.82(1 + 6.3\mu^*),$$

$$\omega_2 = \sqrt{\frac{1}{\lambda} \int_{\omega_{min}}^{\omega_{max}} \left[\frac{2 \cdot a^2 F(\omega)}{\omega} \right] \omega^2 d\omega} \quad (\text{S8})$$

f_1 , f_2 , Λ_1 , Λ_2 are functions and correlation factors, used in Allen-Dynes paper for calculating the critical temperature in the case of the inapplicability of the McMillan approximation for large EPC parameters $\lambda > 2$, ω_2 is square root of the mean squared frequency. Minimal ($\omega_{min} > 0$) and maximal (ω_{max}) frequencies were determined as the extreme zero values of the Eliashberg function, where $a^2F(\omega) < 10^{-6}$.

Electronic properties of Th-H phases

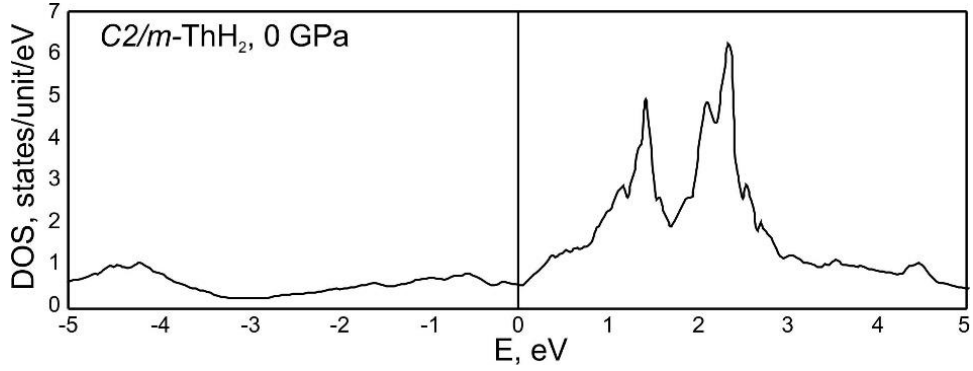


Fig. S5. Electronic density of states of $C2/m$ -ThH₂ phase at 0 GPa. $DOS(E_F) = 0.35$ states/unit/eV

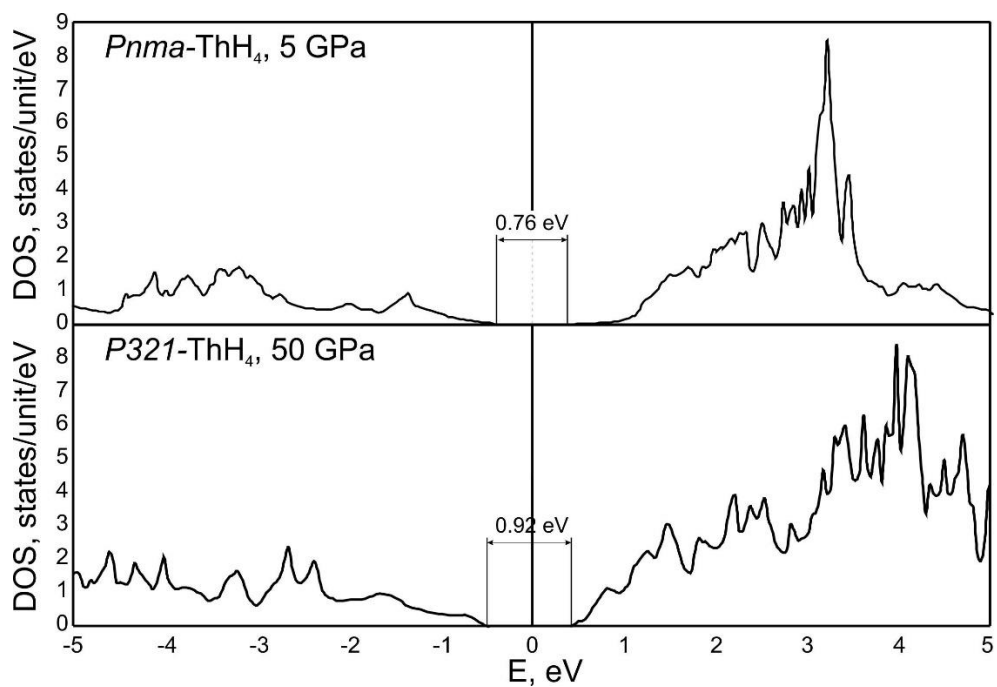


Fig. S6. Electronic densities of states of *Pnma*-ThH₄ and *P321*-ThH₄ phases at 5 and 50 GPa, respectively.

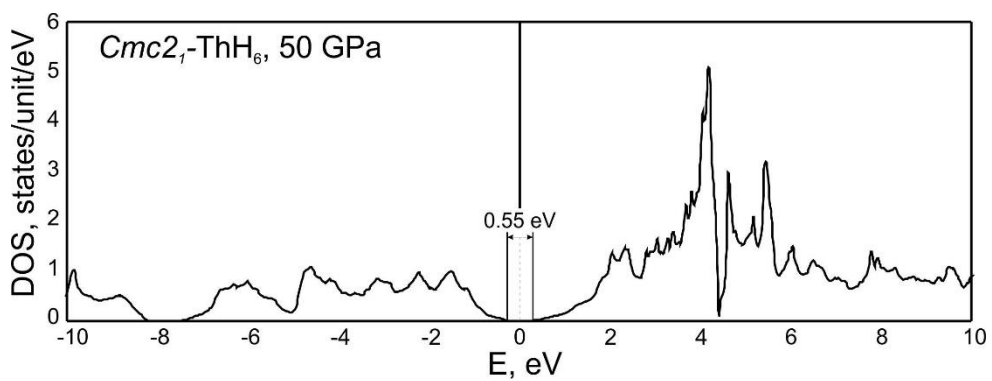


Fig. S7. Electronic density of states of *Cmc2₁*-ThH₆ phase at 50 GPa.

Eliashberg spectral functions for ThH₃, Th₃H₁₀ and ThH₇ phases

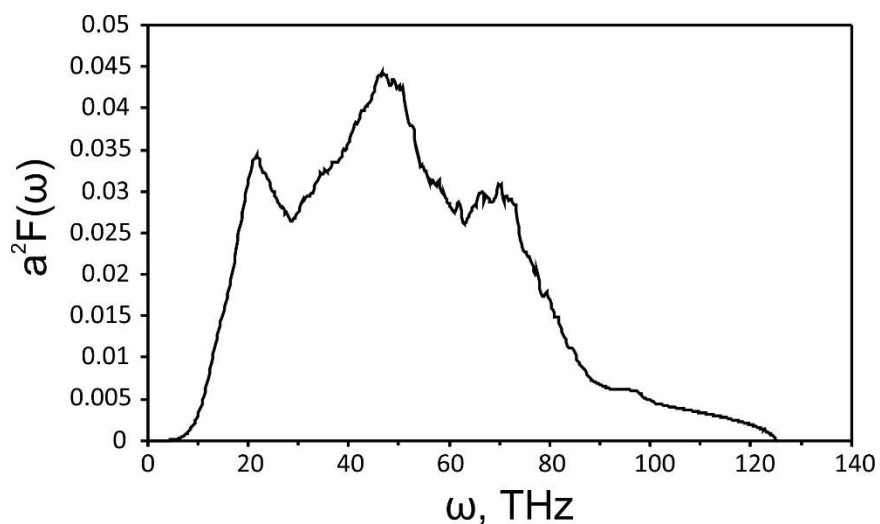


Fig. S8. Eliashberg function $a^2F(\omega)$ of $R\bar{3}m$ -ThH₃ phase at 100 GPa

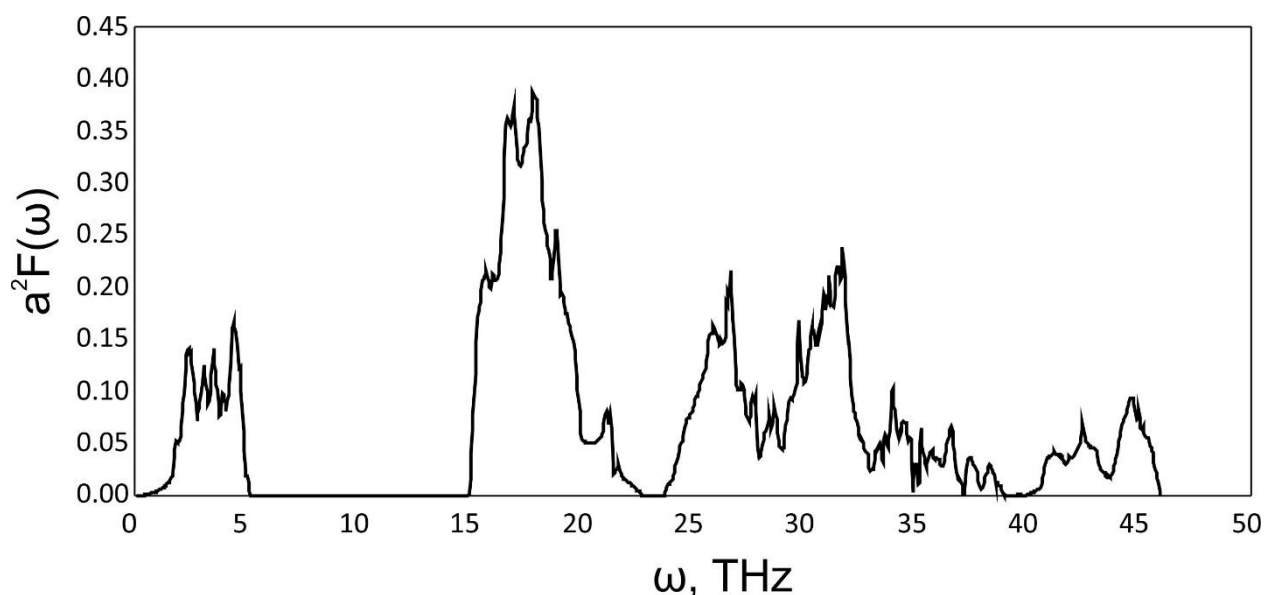


Fig. S9. Eliashberg function $a^2F(\omega)$ of $Immm$ -Th₃H₁₀ phase at 10 GPa

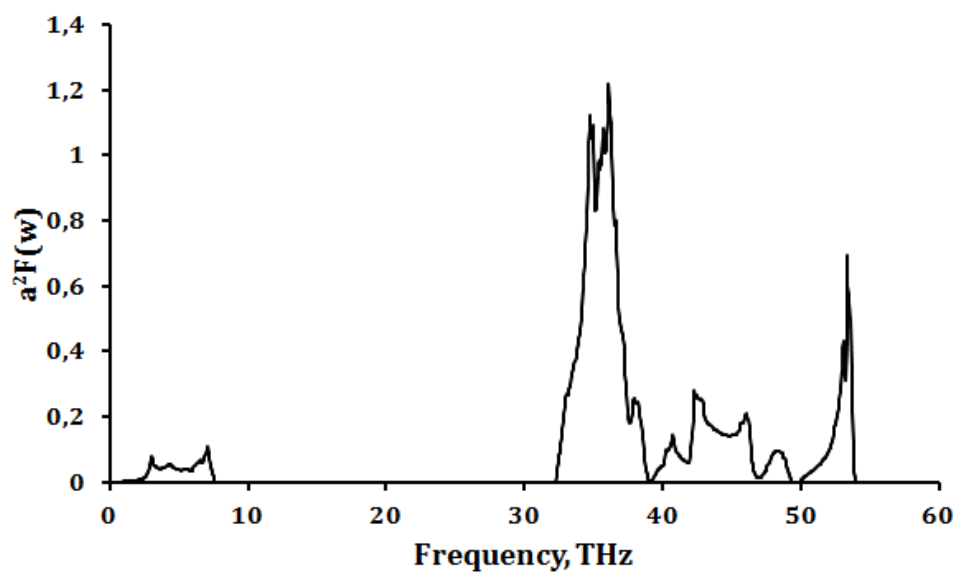


Fig. S10. Eliashberg function $a^2F(\omega)$ of $I4/mmm$ -ThH₄ phase at 85 GPa

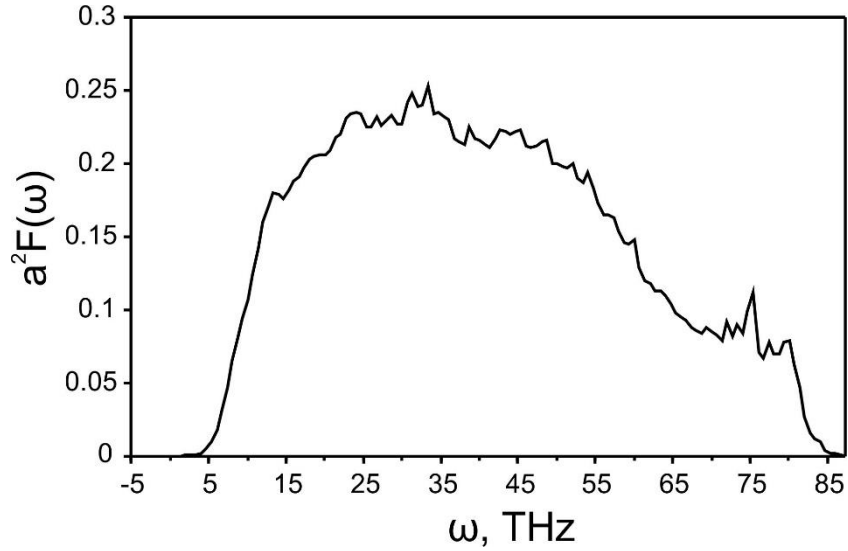


Fig. S11. Eliashberg function $a^2F(\omega)$ of $P2_1/c$ -ThH₇ phase at 100 GPa

Dependence of T_c on the pressure for ThH₁₀ and UH₈ phases

Here we describe a detailed analysis of pressure dependence of T_c of ThH₁₀ phase and UH₈ [2]. Fig. S12a shows the electronic DOS of ThH₁₀ calculated at 100, 200 and 300 GPa, while the densities of states of UH₈ phase at 0, 50 and 100 GPa, are shown in Fig. S12b. All the data for analysis are summarized in Table S2. It is clearly seen from both Table S2 and Fig. S12 that the density of states at Fermi level decreases linearly with pressure for ThH₁₀, while for UH₈ N_f decreases non-monotonically with the minimal density of states at 50 GPa.

Table S2. Calculated data for ThH₁₀ and UH₈ phases

ThH ₁₀						
P, GPa	Cell volume, Å ³	N_f , states/unit/eV	ω_{log} , K	λ	T_c (A-D)*, K	$\ln[T_c/\omega_{log}]$
100	248.8	0.61	1042	2.19	194.3	-1.679
200	205.4	0.53	1215	1.58	163.0	-2.008
300	183.2	0.48	1728	0.99	126.4	-2.615
*Full Allen-Dynes (eq. (1))						
UH ₈						
P, GPa	Cell volume, Å ³	N_f , states/unit/eV	ω_{log} , K	λ	T_c (McM)*, K	$\ln[T_c/\omega_{log}]$
0	5.516	1.02	1403	1.88	193.2	-1.98
50	5.158	0.38	1594	1.29	156.7	-2.32
100	4.962	0.6	1933	0.94	122.4	-2.76
*Modified McMillan (eq. (2))						

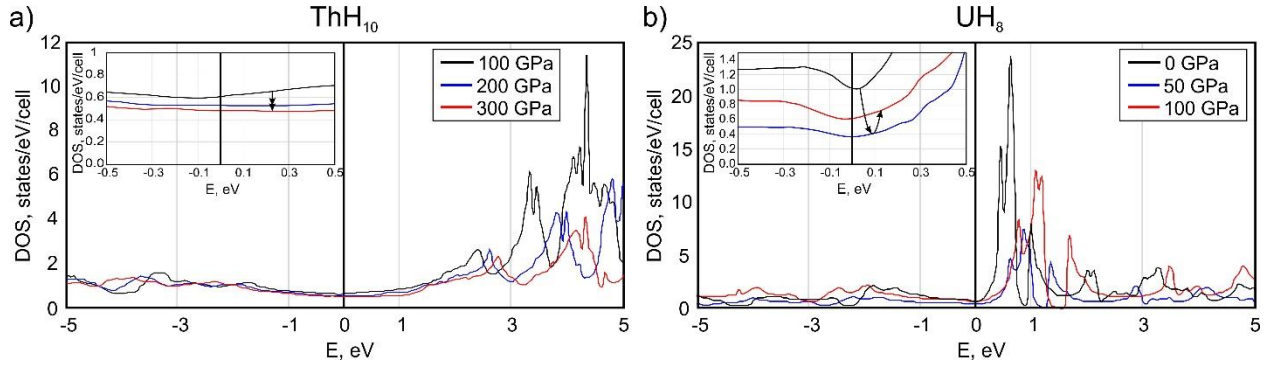


Fig. S12. Electronic densities of states of a) ThH₁₀ and b) UH₈ as a function of pressure. Fermi level is set to zero. Inset shows zoomed region from -0.5 to 0.5 eV for better view of DOS at Fermi level.

Results for ThH₁₀ and UH₈ [2] show linear dependence of logarithmic frequency on pressure which can be well described by the following formula:

$$\gamma = \left(\frac{\partial \ln(\omega)}{\partial \ln(V)} \right)_T, \quad (\text{S9})$$

where γ is the Grüneisen parameter, showing only small dependence on pressure and for most materials equal to ~ 1 -1.5.

Calculated gradient of the critical temperature dependence dT_C/dP for ThH₁₀ phase is negative as for the majority of metals and equals to $-3.1 \cdot 10^{-5}$ K/atm at 100 GPa. This value is similar to values for low- T_C superconducting metals like Hg, Ga, Bi-II [3]. This value is also similar to that of CaH₆ phase from Ref. [4] where the $dT_C/dP = -3.34 \cdot 10^{-5}$ K/atm. For UH₈ $dT_C/dP = -7.08 \cdot 10^{-5}$ K/atm is two times higher, which is a kind of anomaly. Similarity of pressure dependence of T_C for ThH₁₀ with other metals opens a new way of using the well-known empirical equation for low- T_C superconductors:

$$-\ln \left(\frac{T_C}{\omega_{log}} \right) = C v^{-\varphi}, C > 0 \quad (\text{S10})$$

with constant C and φ calculated earlier for non-transition metals ($\varphi = 2.5 \pm 0.6$) [5,6]. From calculated data (interpolation of $\ln[T_C/\omega_{log}]$ function by a $\times v^b$ law) we can directly determine the coefficients $\varphi = 1.395$, $C = 3594.4$ ($R^2 = 0.94$), see Table S2. For UH₈ we obtained much lower values $\varphi = 1.012$, $C = 349.3$ ($R^2 = 0.97$), see Table S2.

Using the modified McMillan equation (see eq. (2)) we derived the dependence of the EPC coefficient on the pressure as:

$$T_C = \frac{\omega_{log}}{1.2} \exp \left(\frac{-1.04(1 + \lambda)}{\lambda - \mu^* - 0.62\lambda\mu^*} \right)$$

$$\ln \left(\frac{T_C}{\omega_{log}} \right) = \ln \left(\frac{1}{1.2} \right) + \left(\frac{-1.04(1 + \lambda)}{\lambda - \mu^* - 0.62\lambda\mu^*} \right) \Bigg|_{\mu^*=0.1} \rightarrow 0.1823 + \frac{1.04(1 + \lambda)}{0.938\lambda - 0.1} \quad (\text{S11})$$

$$= C v^{-\varphi}$$

As a result, we obtained the following equation:

$$\lambda(P) = 0.1066 \times \frac{C v^{-\varphi} + 10.22}{C v^{-\varphi} - 1.291} \quad (\text{S12})$$

For better comparison we summarized the obtained data in the Table S3 and show it in Fig. S13.

Table S3. Comparison of numerical and analytical results for ThH₁₀ and UH₈

ThH ₁₀				
P, GPa	T _C (QE), K	T _C (eq. (S10)), K	λ (QE)	λ (eq. (S12)) (μ* = 0.1, φ(McM) = 1.35)*
100	194.3	188.1	2.19	2.24
200	163.0	164.2	1.58	1.33
300	126.4	127.2	0.99	0.89
UH ₈				
0	193.2	190.6	1.88	1.87
50	156.7	160.0	1.29	1.30
100	122.4	124.0	0.94	0.95

*φ(McM) – is φ based on modified McMillan calculation of T_C.

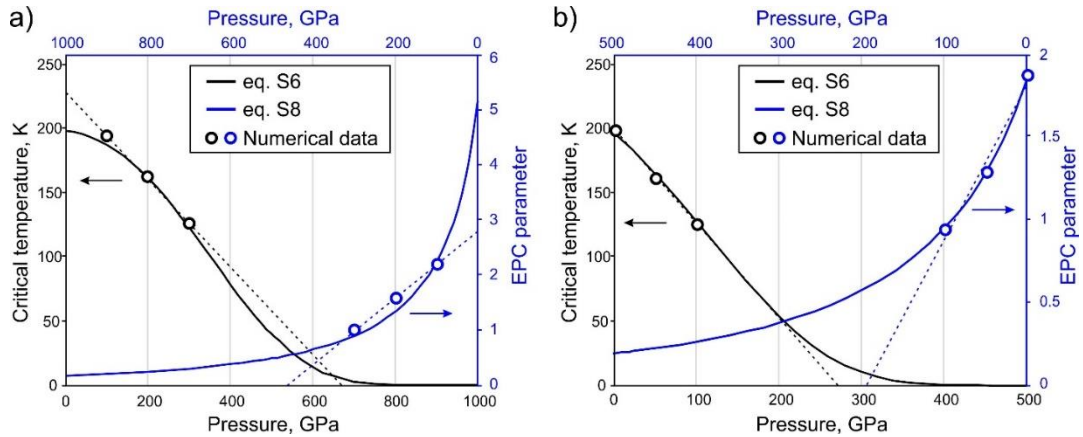


Fig. S13. Analytical dependence for T_C (eq. S6) and λ (eq. S8) as a function of pressure compared to numerical data (calculated by QE data) of a) ThH₁₀ and b) UH₈ phases

As one can see from Fig. S13a the linear dependence of T_C of ThH₁₀ on pressure is valid only within the pressure range 150-300 GPa. At low-pressure region analytical eq. (S10) deviates from linear law. Critical temperature decreases with pressure and approaches 0 at ~900 GPa, while linear approximation of numerical data gives lower value of 675 GPa. The EPC parameter calculated using analytical eq. (S12) also decreases nonlinearly with pressure. Results for UH₈ are shown in Fig. S13b. Here one can see good agreement between analytical and numerical data. The T_C behaves almost linearly in the pressure region 0-200 GPa, which is also confirmed by calculations.

References

- [1] P. B. Allen and R. C. Dynes, Phys. Rev. B **12**, 905 (1975).
- [2] I. A. Kruglov, A. G. Kvashnin, A. F. Goncharov, A. R. Oganov, S. Lobanov, N. Holtgrewe, and A. V. Yanilkin, arXiv:1708.05251 <https://arxiv.org/abs/1708.05251>, (2017).
- [3] N. B. Brandt and N. I. Ginzburg, Sov. Phys. Uspekhi **12**, 344 (1969).
- [4] H. Wang, J. S. Tse, K. Tanaka, T. Iitaka, and Y. Ma, Proc. Natl. Acad. Sci. **109**, 6463 (2012).
- [5] H. Rohrer, Helv Phys Acta **33**, 675 (1960).
- [6] J. L. Olsen and H. Rohrer, Helv Phys Acta **33**, 872 (1960).